Cellular Microbiology (2012) **14**(7), 983–993
doi:10.1111/j.1462-5822.2012.01786.x
First published online 12 April 2012

Host cell deformability is linked to transmission in the human malaria parasite *Plasmodium falciparum*

Mythili Aingaran,[1†] Rou Zhang,[2†] Sue KaYee Law,[1†] Zhangli Peng,[3†] Andreas Undisz,[3] Evan Meyer,[1] Monica Diez-Silva,[3] Thomas A. Burke,[1] Tobias Spielmann,[4] Chwee Teck Lim,[2] Subra Suresh,[3] Ming Dao[3*] and Matthias Marti[1*]

[1]*Department of Immunology and Infectious Diseases, Harvard School of Public Health, Boston, MA 02115, USA.*

[2]*Singapore-MIT Alliance, National University of Singapore, 4 Engineering Drive 3, Singapore 117576.*

[3]*Department of Materials Science and Engineering, Massachusetts Institute of Technology, Cambridge, MA 02139, USA.*

[4]*Bernhard Nocht Institute for Tropical Medicine, Hamburg, Germany.*

Summary

Gametocyte maturation in *Plasmodium falciparum* is a critical step in the transmission of malaria. While the majority of parasites proliferate asexually in red blood cells, a small fraction of parasites undergo sexual conversion and mature over 2 weeks to become competent for transmission to a mosquito vector. Immature gametocytes sequester in deep tissues while mature stages must be able to circulate, pass the spleen and present themselves to the mosquito vector in order to complete transmission. Sequestration of asexual red blood cell stage parasites has been investigated in great detail. These studies have demonstrated that induction of cytoadherence properties through specific receptor–ligand interactions coincides with a significant increase in host cell stiffness. In contrast, the adherence and biophysical properties of gametocyte-infected red blood cells have not been studied systematically. Utilizing a transgenic line for 3D live imaging, *in vitro* capillary assays and 3D finite element whole cell modelling, we studied the role of cellular deformability in determining the circulatory characteristics of gametocytes. Our analysis shows that the red blood cell deformability of immature gametocytes displays an overall decrease followed by rapid restoration in mature gametocytes. Intriguingly, simulations suggest that along with deformability variations, the morphological changes of the parasite may play an important role in tissue distribution *in vivo*. Taken together, we present a model, which suggests that mature but not immature gametocytes circulate in the peripheral blood for uptake in the mosquito blood meal and transmission to another human host thus ensuring long-term survival of the parasite.

Received 4 February, 2012; revised 6 March, 2012; accepted 7 March, 2012. *For correspondence. E-mail mmarti@hsph.harvard.edu; Tel. (+1) 617 432 4126; Fax (+1) 617 738 4914 or E-mail mingdao@mit.edu; Tel. (+1) 253 2100; Fax (+1) 258 0390.
†These authors contributed equally to this work.

Introduction

Malaria continues to be a major public health concern worldwide with over 200 million infections and 665 000 deaths annually (Murray *et al.*, 2012). *Plasmodium falciparum*, the parasite that is responsible for most of the mortality related to human malaria, has been able to evade eradication despite decades of innovative intervention strategies. As parasites rapidly develop resistance to new drugs and employ various means of immune evasion, it has become clear that successful eradication may hinge upon targeting multiple life cycle stages. As a result there has been renewed interest in understanding key features of gametocyte development. Like all *Plasmodium* parasites, *P. falciparum* invades red blood cells (RBCs) and undergoes asexual replication within them. This proliferation phase leads to a large fraction of infected RBCs, which is the major cause of the pathology of falciparum malaria. A small percentage of parasites undergo sexual conversion to form gametocytes in a process that takes about 10–14 days. While gametocytes are not thought to contribute to any clinical symptoms they are responsible for transmission to the *Anopheles* mosquito.

Historically, five gametocyte stages have been defined in *P. falciparum* based on the staining properties in Giemsa smears (Hawking *et al.*, 1971). Stage I is rounded while the mature Stage V is elongated and adopts a falciform shape. Clinical studies have demonstrated that only Stage V gametocytes appear in peripheral blood

smears except in some splenectomized patients or following certain drug treatments where immature forms have been detected (Bachmann *et al*., 2009). Similarly, asexual trophozoite and schizont stages can be found under these conditions. These findings suggest that all gametocyte stages can circulate if they are not retained in the spleen or actively sequestered. Indeed, studies have suggested that developing transmission stages sequester in bone marrow and spleen (Thomson and Robertson, 1935; Smalley *et al*., 1981). However, a comprehensive analysis of gametocyte enrichment across tissues and stages is lacking so far. Similarly, underlying mechanisms of sequestration have remained elusive but evidence suggests that knobs are mostly absent in gametocytes and the major receptor–ligand interactions found in asexual stages do not have key roles in this process (Rogers *et al*., 1996; Hayward *et al*., 1999). It is therefore plausible that mechanical entrapment based on altered RBC deformability could contribute to the tissue enrichment of developing gametocytes and their eventual release into circulation.

In asexually replicating *P. falciparum* parasites sequestration depends on extensive remodelling of the host RBC, which leads to both severe decrease in cellular deformability and strong cytoadherence to endothelial cells (Glenister *et al*., 2002; Suresh *et al*., 2005; Park *et al*., 2008). Because mechanically altered RBCs are recognized and retained in the spleen, sequestration is important in order to avoid splenic clearance. Various biomechanical and imaging strategies have provided precise measures of deformability of asexual stages and shown that the deformability decreases approximately 20-fold as rings mature to the schizont stage (Nash *et al*., 1989; Suresh *et al*., 2005; Mills *et al*., 2007). Only the ring stages are sufficiently deformable to traverse splenic endothelial slits. In contrast, iRBCs infected with all stages of the related human malaria parasite *Plasmodium vivax* remain similarly deformable, thereby providing an explanation for their ability to pass the spleen without sequestering in deep tissues (Handayani *et al*., 2009).

We have investigated cell deformability properties of *P. falciparum* during sexual development and observed a decrease in both host RBC membrane and parasite deformability as the gametocyte matures from Stage I to IV followed by a restoration of deformability in Stage V. Remarkably, our experiments and simulations also suggest that only Stage V gametocytes, but not Stage IV or earlier gametocyte stages, may easily traverse through splenic endothelial slits under physiological pressure. Based on these findings, we propose a model that captures the critical role played by the spleen in ensuring that transmission competent Stage V gametocytes are present in the circulating blood.

Results

Establishment of a transgenic line for live analysis of sexual development in P. falciparum

Gametocyte development in *P. falciparum*, which is marked by a series of distinct morphological transformations that occur over approximately 2 weeks, is slower than in other malaria parasites. Early sexual stages (Stage I) are visually difficult to distinguish from asexual stages without labelling with stage-specific markers. After 2 days, parasites adopt an elongated shape and are marked by a sub-pellicular cytoskeleton (Stage II). There is further elongation (Stage III and Stage IV) until final maturation into mature male (sausage shaped) and female (crescent shaped) gametocytes (Stage V). The relative scarcity in the peripheral circulation of the human host and in *in vitro* culture systems represents a challenge for detection and analysis. Our first goal was to generate a transgenic parasite line with strong reporter expression throughout sexual development to allow unambiguous identification of all gametocyte stages in live cells. Such a line would be a very useful asset for further characterization of gametocyte-specific processes in single cell assays. We recently generated a series of transgenic parasite lines expressing a fluorescent reporter under gametocyte-specific promoters (Buchholz *et al*., 2011). These lines were generated in a 3D7 clone that has a sexual conversion rate of approximately 2%. It produces viable Stage V gametocytes that are capable of developing into male microgametes and female macrogametes under *in vitro* conditions. In order to achieve maximum fluorescence reporter intensity and minimal autofluorescence, we generated in the same background an additional transgenic line expressing a tandem red fluorescence protein termed tandem Tomato (TdTom) under the strongest of the three promoters. This promoter is naturally controlling the *PF10_0164* gene encoding the highly expressed and stage-specific membrane protein Etramp 10.2 (Spielmann *et al*., 2003; Silvestrini *et al*., 2005). Analysis of the transgenic line named 164/TdTomato by epifluorescence microscopy revealed strong cytoplasmic TdTomato expression throughout sexual development (Fig. 1). For these and all the following experiments, parasite staging was done according to the definitions by Hawking *et al*. (Hawking *et al*., 1971) and Sinden (Sinden, 1982), as described in the legend to Fig. 1.

Analysis of key parameters by 3D imaging

Shape is often critically important in evaluating a cell's overall deformability (Diez-Silva *et al*., 2010). Utilizing the 164/TdTomato parasites our next aim was to generate three-dimensional images to measure key parameters

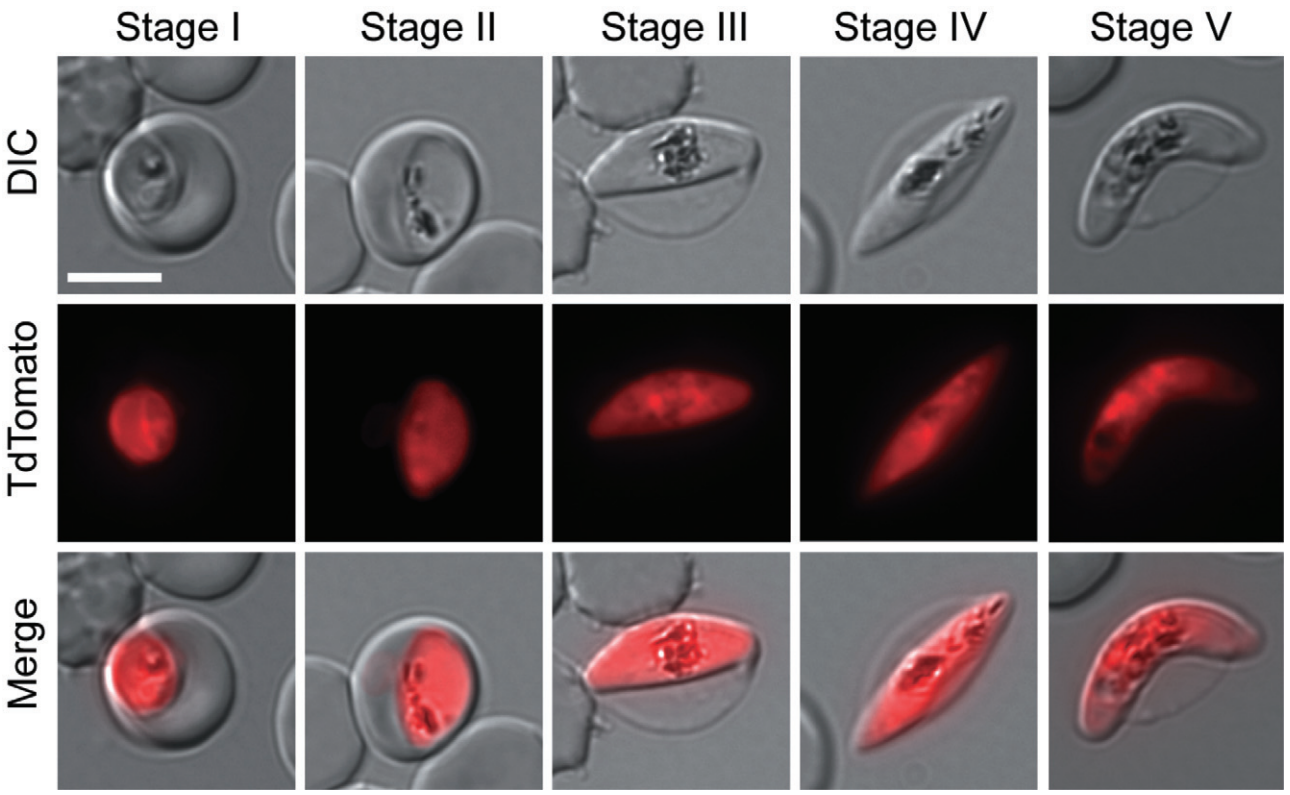

Fig. 1. Gametocyte development in the transgenic 164/TdTomato line. Shown are representative cells for each developmental stage as defined previously by Hawking *et al.* (Hawking *et al.*, 1971) and Sinden (Sinden, 1982). Stage I emerges 30 h post invasion (pi). It is indistinguishable from the young asexual trophozoite by light microscopy. We defined Stage I parasite by shape and the presence of TdTomato fluorescence. Stage II emerges 48–72 h pi. We defined early Stage II parasites by the oat grain like morphology and later Stage II by the D-shaped morphology. Stage III emerges 3–5 days pi. We defined Stage III parasites by the relative elongation/flattened D-shape compared with late Stage II. Later Stage III parasites were defined by the presence of lightly pointed ends. Stage IV emerges 6–8 days pi. These parasites were defined by the spindle shape and axial symmetry with two pointed ends. Stage V emerges 10–14 days pi. This stage is mainly defined by the crescent female morphology, while the male Stage V gametocyte requires additional markers for unambiguous staging. Because male Stage V gametocytes only make up 15–20% of all Stage V gametocytes, we defined Stage V by the easily recognizable crescent shape of the female Stage V. For each cell an epifluorescence image with TdTomato distribution, differential interference contrast (DIC) and a merge of the two are shown. Images were collected at ambient temperature with a Zeiss Axioscope microscope using a 100×/1.4 immersion oil lens, and captured using a Hamamatsu Orca C4742-95 camera. Acquisition software Zeiss Axiovision was used.

that influence deformability. Specifically, this entailed definition of the shape of the parasite and host cell by measuring the maximal expansion in all three dimensions, and to calculate the surface area to volume ratio of each stage. We captured at least 10 cells from each sexual stage by confocal microscopy of live cells to generate three-dimensional reconstructions of iRBCs (Fig. 2A and Supporting Videos S4–S18). Importantly, the RBC membrane was labelled with BODIPY-FLC5-Ceramide in order to mark its outline for proper calculation of host parameters (Fig. 2A). These measurements support the observation that morphological differentiation of the parasite causes significant deformation of the host cell in transforming from a discoidal to an elongated elliptical shape. Starting at Stage II, the elongation of the parasite alters the natural shape of a RBC, thereby stretching and elongating it to maximum length at Stage IV with a corresponding decrease in width. Parasite and host cell reach a maximum average length in Stage IV of 11.4 ± 1.3 μm and 12 ± 1.4 μm, respectively, and a width of 3.5 ± 0.6 μm and 4.6 ± 0.7 μm respectively (Fig. 2B and Table S3). This results in a change in aspect ratio from close to 1 for both the parasite and host in Stage I to 3.2 and 2.6, respectively, in Stage IV.

Human RBCs have a volume of about 90 fl with a surface membrane area of about 136 μm^2. They can swell up to a spherical shape containing 150 fl of volume without membrane distension (Fung, 1993). Aging RBCs show a decrease in both surface membrane area and volume of up to 10% compared with young controls, probably due to the continuous release of membrane particles during circulation and splenic passage (Waugh *et al.*, 1992). We calculated the surface area and volume of parasite and host cell from five individual cells per stage. These measurements demonstrate that there is no significant change in both surface area and volume of the host

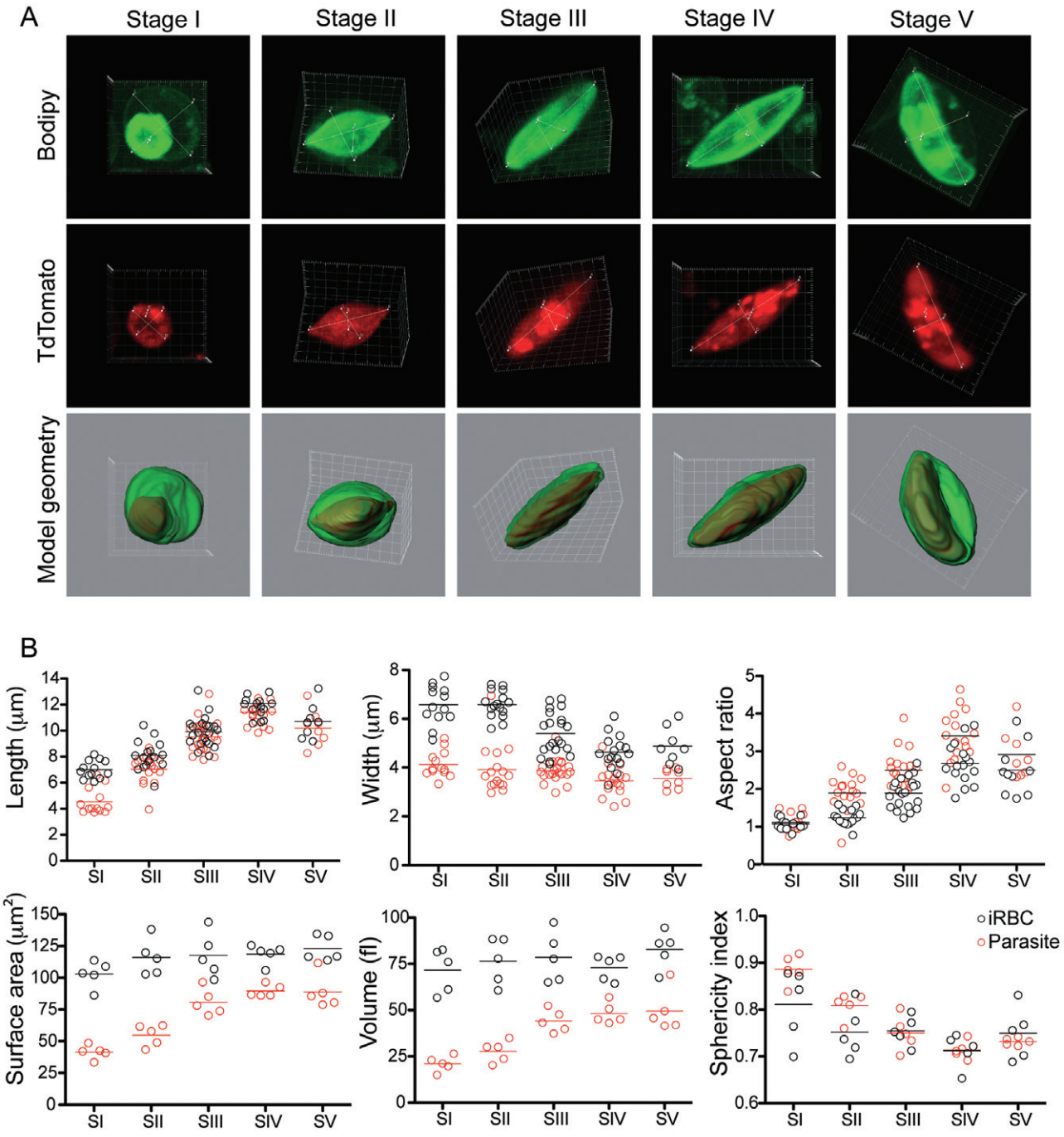

Fig. 2. 3D analysis and key parameters during sexual development.
A. Gametocyte development in three dimensions. Shown is one representative cell per stage. Each cell is shown as a maximum projection; red (TdTom), green (Bodipy-FL5- Ceramide) and as a surface rendered merge of the two channels. Measurements for aspect ratios are included. Movies of the original files for each cell shown are available as *Supporting information*. Images were taken using an Olympus FV1000 confocal microscope equipped with a 100×/1.4 oil immersion lens and stacks collected using Fluoview software. Three-dimensional images were constructed using the Imaris software.
B. Calculation of vital parameters. Length (x), width (y) and thickness (z) dimensions were measured from $n = 13$ (Stage I), $n = 16$ (Stage II), $n = 21$ (Stage III), $n = 15$ (Stage IV) and $n = 8$ (Stage V). The complete data set is available as Table S3.

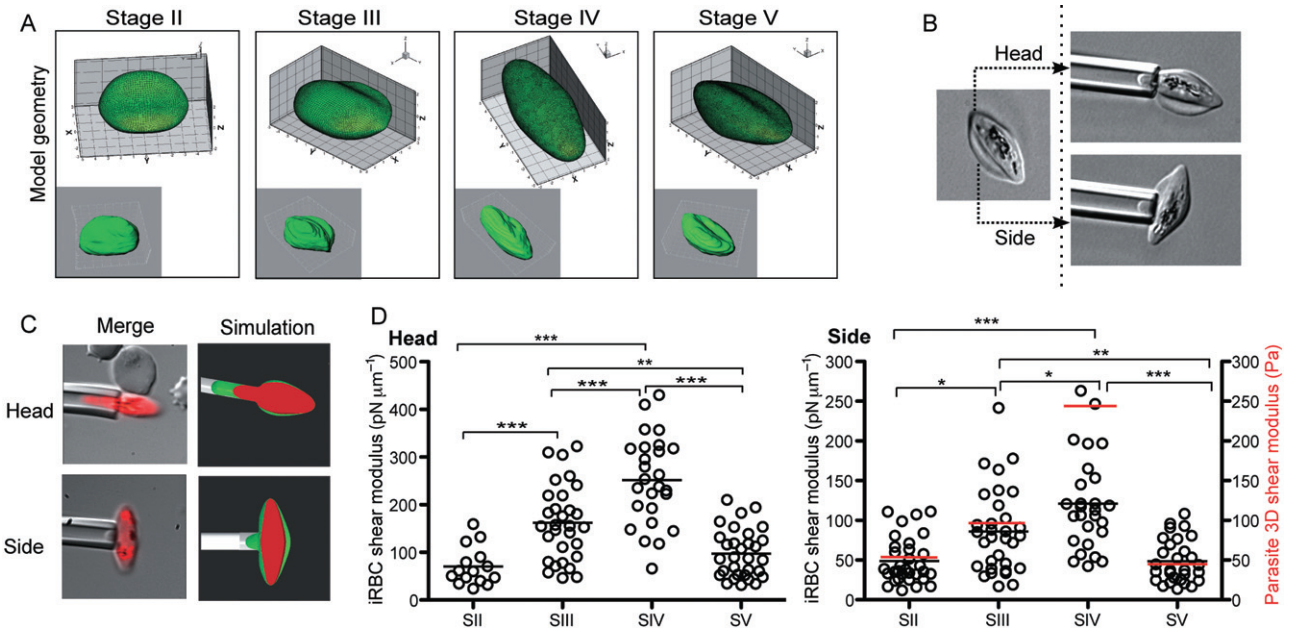

Fig. 3. Micropipette aspiration assays in developing gametocytes.
A. Definition of cell shape. For each stage the 3D reconstruction of a representative cell was used to calculate the geometry of the iRBC as a correlate for cell shape.
B and C. Schematic of capillary measurements. In order to account for the irregular shape of gametocyte-infected RBCs, the cell was aspired from side and head separately. In addition, a fluorescence image of the iRBC was captured at the end-point of the assay.
D. Side and head shear modulus calculations and parasite rigidity. Shown are individual data points and mean for each stage. Average parasite rigidity is shown as a red bar in the side shear modulus graph. After ensuring that the data for each stage did not deviate severely from normality and that the assumptions for ANOVA are met, we performed a one-way ANOVA, followed by Turkey's HSD procedure to test the difference between each pair of stages. The final *P*-values from this test are given by $*P < 0.005$; $**P < 0.001$; $***P < 0.0005$.

cell, despite the significant change in cell shape caused by the parasite (Fig. 2B). The range of the two parameters during sexual development is also similar to the numbers obtained in a previous study for RBCs infected with asexual parasites (Esposito *et al*., 2010). On the other hand, the parasite grows significantly in both volume and surface area from Stage I to Stage IV, but still maintains its surface area-to-volume ratio similar to that of the host cell. These data suggest that while the actual shape may play a critical function any changes in deformability during sexual development cannot be attributed to a change in the surface area to volume ratio of the host cell.

Initial decrease in iRBC deformability is followed by a rapid restoration at the onset of mature Stage V gametocytes

The ability of healthy RBCs to deliver oxygen to tissues depends on their capacity to undergo repeated deformations in circulation. This requires navigation through the smallest capillaries, which are estimated to be on the order of 4–10 μm in diameter (Krause, 2005). Similarly, mature gametocytes have to circulate to achieve their function. To directly measure potential changes in cellular deformability as gametocytes mature, we evaluated the shear modulus of different stages. Micropipette aspiration was the best technique for such an analysis because it allows measurements to be performed from different orientations, which is essential especially when cells are elongated. In addition, when there is difficulty obtaining pure populations of each stage, this technique allows measurement of individual cells. Due to the elongated shape of Stages II–V iRBCs, we measured the shear modulus both along the longitudinal and transverse axes. If possible, the second measurement was taken in duplicate, from two opposing sides of the RBC membrane (see schematic Fig. 3). Given the asymmetric shape of both host RBC and parasite we used the stage-specific geometric shape in finite element method (FEM) simulations to calculate the membrane shear modulus. Ignoring the influence of parasite for now, with both side and head measurements we found a significant increase in shear modulus (i.e. a significant decrease in deformability) during gametocyte development from Stage II–IV, followed by a sharp drop in shear modulus from Stage IV to Stage V (Fig. 3C/D). Careful FEM modelling showed that the parasite has negligible influence towards the estimated host RBC membrane shear modulus in the side measurements, whereas influences of parasite in the head experiments can be used to estimate the

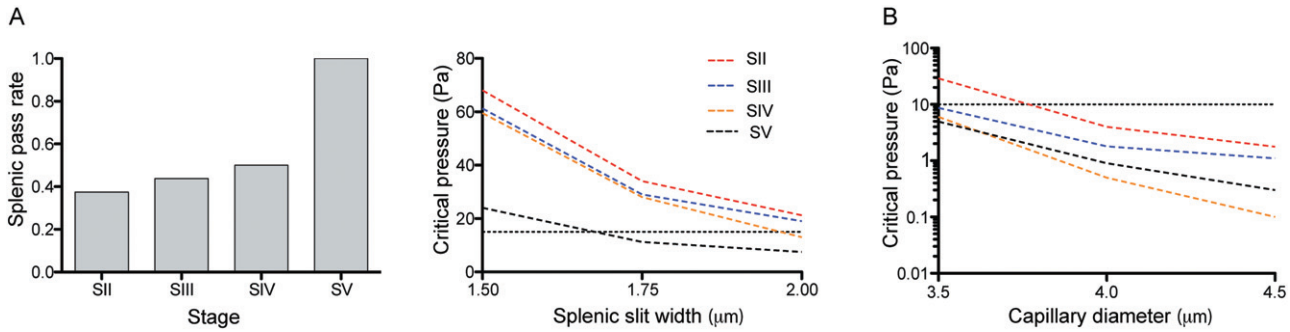

Fig. 4. Simulating *in vivo* behaviour of malaria transmission stages.
A. Parametric study to simulate splenic passage of developing gametocytes. Cell shape, deformability and parasite rigidity as well as the geometry of the splenic slit was used to calculate the rate of splenic passage for each gametocyte stage (left panel). Slit width was varied from 1.5 to 2 μm and pressure drop per cell from 0 to 80 Pa. If we take the physiological pressure drop per cell as 15 Pa (dashed line), and the limiting splenic slit width as 2 μm, under these conditions the majority of immature gametocytes cannot pass. Both slit width and critical pressure are contributing to the pass rate (right panel).
B. Simulation of microcirculation. Capillary diameter was varied from 3.5 to 4.5 μm, and pressure drop per cell from 0 to 30 Pa. Under physiological flow (10 Pa pressure drop per cell, dashed line) all gametocyte stages can pass through the microcirculation at a minimal capillary diameter of 4 μm.

stage-dependent parasite rigidity. Stage IV parasites were found to possess the highest rigidity (Fig. 3B). These results are consistent with a recent paper suggesting that Stage V gametocytes are more deformable than immature gametocytes when deformability was measured by ektacytometry (Dearnley *et al*., 2012).

Passage of Stage V gametocytes through endothelial slits in the venous sinus of the spleen

To investigate the physiological relevance of our observed alterations in host RBC shear modulus and parasite rigidity during gametocyte maturation, we utilized three-dimensional whole cell FEM simulations to predict whether their shape and deformability characteristics allowed passage through the spleen and capillaries. For the simulations we used our extracted cell geometry, host RBC shear modulus and parasite rigidity data, as well as published dimensions for the splenic endothelial slits and minimal capillary diameter (Cokelet, 1981; Krause, 2005). Our simulations suggest that Stage V gametocytes can efficiently pass the spleen under physiological pressure (Fig. 4A). Comparison of Stage II and Stage V cells, which had similar shear modulus values, showed that only Stage V could pass under physiological pressure. The reason is that Stage V cells are generally much more slender (~ 32% longer longitudinally and ~ 28% smaller in transverse cross-section, Table S3) than Stage II cells despite similar volumes and surface areas between these two stages. Based on the 3D confocal measurements shown in Table S3, and assuming an elliptical cross-sectional shape, Stage II have an average cross-sectional areas of 62.4 μm^2 while this area is only 45.1 μm^2 for Stage V. Our simulations therefore suggest that splenic gametocyte passage is quite sensitive to the transverse cross-sectional area. This also explains why some immature Stage III and IV gametocytes are predicted to pass without deformation, as their dimensions are smaller than that of the splenic slit. Next, we performed simulations to evaluate the critical pressure for iRBCs to pass the smallest capillaries with a 4 μm diameter in microcirculation (Fig. 4B). These careful simulations predict that all gametocyte stages can pass these 4 μm diameter smallest capillaries under physiological pressure (~ 10 Pa). Altogether our data suggest that during infection, efficient gametocyte passage through the slow circulation of the spleen and the microcirculation is dependent on a combination of cell size, shape, host RBC shear modulus and parasite rigidity. In addition, the shape of the size limiting pores in capillary and spleen, i.e. tubular versus slit shape respectively, is an important factor in determining the critical cell passage conditions.

Discussion

A critical feature of the *P. falciparum* life cycle is the efficient transmission of gametocytes from an infected patient to its mosquito vector. The parasite invests in a gametocyte development path that takes much longer than the asexual cycle and undergoes characteristic morphological changes along the way. Strikingly, the parasite is transmitted efficiently despite the presence of relatively few Stage V gametocytes in the peripheral circulation of the human host. As for any other cells in circulation, mature gametocytes require a certain degree of cell deformability in order to navigate through the splenic endothelial slits and capillaries. In fact one of the mechanisms by which the splenic reticuloendothelial system clears iRBCs is by detecting a decrease in overall cell deformability (Deplaine *et al*., 2011). To understand why

only mature gametocytes circulate, we took a stepwise approach to dissecting the parameters that could contribute to their overall deformability properties.

First, to perform assays on individual gametocytes we developed a fluorescent transgenic line that allows definition and tracking of all gametocyte stages in live cells. This is expected to be a useful tool as a quantitative gametocyte characterization assay due to its ability for continuous live cell imaging during parasite development. Because any phenotypic characterization during sexual development relies on proper assignment of stages, we captured morphological differentiation in as much detail as possible in a series of images, using stage characteristics as defined previously (Hawking *et al*., 1971; Sinden, 1982) and described in the legend to Fig. 1. It is worth mentioning that gametocyte stage development is a continuum with cells transitioning from one stage to another, likely resulting in increased noise when quantifying phenotypes across stages.

Thereafter, we sought to specify the dimensions of each stage as shape and size changes play an important role in determining the overall cellular deformability. Additionally, these images served as a template for tracing the three dimensional outline of each cell for our simulations. Surprisingly, this first detailed analysis of cell geometry in live cells during sexual development revealed the surface area to volume ratio was nearly constant despite the significant changes of the parasite and resultant deformation of the host cell. The overall values for the volume of our live parasites and host cells were in a similar range to recently published measurements in cryopreserved parasites (Hanssen *et al*., 2011), except that we did not observe any significant dip in the volumes of Stage IV gametocytes and host cells. This difference might be due to the use of live parasites as opposed to cryopreserved ones. Based on these results we concluded that the surface area to volume ratio is not a key determinant in the overall deformability changes.

Next, we sought to systematically analyse changes in membrane shear modulus of the host cell during sexual development. Given the difficulty in obtaining pure populations of each gametocyte stage, we chose a single cell approach rather than a population-based analysis. Our method of choice was micropipette aspiration because it also allows individual cell measurements at different orientations, which is critical when iRBCs adopt an asymmetric shape. Specifically, our experiments revealed peak rigidity levels for both host RBC membrane and parasite at Stage IV. In addition, there was a significant drop in rigidity for Stage V gametocytes suggesting this change plays a role in its circulation. As expected, there is scatter among the measurements, which partly could be due to assigning stages when there are gradual changes that occur along the 2-week continuum of structural changes. We noted that there were cells with stage characteristics as defined previously (Hawking *et al*., 1971; Sinden, 1982) while others had shared attributes and were likely transitioning from one stage to the next. As differentiation between male and female gametocytes based only on morphology in the absence of ultrastructural features or marker antibodies is difficult, we defined the mature Stage V gametocytes by the crescent shape, which is characteristic of the female form. Recognizing these aspects we ensured we had clear criteria for staging (see Fig. 1) and had multiple researchers independently identify and assign stages so as to reduce subjective bias. It is also important to note that these measurements were made in the culture-adapted reference strain 3D7. In the future, it will be important to compare multiple strains, including non-culture adapted field isolates, to determine the variability of the observed deformability changes in different genetic backgrounds and immunological settings.

Finally, utilizing the stage-specific shape, dimensions, host RBC shear modulus and parasite rigidity of each gametocyte, we simulated circulatory properties of the iRBC in the splenic slits and capillaries. Remarkably, our simulations revealed that the vast majority of immature gametocytes would be retained in the spleen, while Stage V gametocytes could efficiently pass. Our results suggest that immature gametocytes can circulate if given the opportunity, but that the spleen effectively traps them. This result is supported by previous observations of immature *P. falciparum* gametocytes and asexual trophozoites and schizonts in circulation in splenectomized patients and non-primate monkeys [i.e. (Bachmann *et al*., 2009)]. In asexual stage parasites, it has been shown that splenic passage is required for the efficient binding of iRBCs to endothelial cells (David *et al*., 1983). Previous studies suggest that immature gametocytes sequester not only in the spleen but also in the bone marrow (Thomson and Robertson, 1935; Smalley *et al*., 1981). Therefore, the role of additional factors besides deformability and splenic clearance in determining tissue-specific sequestration needs to be explored.

The mechanistic basis for the observed deformability changes remains to be investigated. It is likely that exported parasite proteins contribute to the initial decrease in host cell deformability during sexual development. Multiple secreted parasite proteins have previously been implicated in regulating host RBC deformability in asexual stages, including the DnaJ proteins RESA and MESA (Maier *et al*., 2008). Some of these proteins increase the rigidity of the host cytoskeleton and anchor it to the parasite-induced knob structures on the iRBC surface, thereby linking the decrease in RBC deformability to an increase in cytoadherence (Mills *et al*., 2007). A recent proteomic analysis of early gametocyte development demonstrated an enrichment of exported proteins,

including DnaJ proteins, in these stages (Silvestrini *et al*., 2010). However, the process is not entirely analogous to the asexual stages because of the absence of a major role for asexual-like receptor–ligand interactions involved in cytoadherence (Rogers *et al*., 1996; Hayward *et al*., 1999). Moreover, the restoration of deformability of mature Stage V gametocytes must be a process unique to the sexual cycle, as the end-point of the asexual cycle is the egress of progeny merozoites from the bursting schizont. A decrease in parasite rigidity, as observed in our experiments, could also contribute to the restoration of deformability in Stage V. This is also consistent with earlier ultrastructural images showing the disappearance of the peripheral parasite cytoskeleton in the Stage V gametocyte (Sinden, 1982). Further investigations are required to delineate the parasite determinants for deformability changes in gametocytes.

Overall, our work represents the first analysis of biomechanical properties of individual gametocytes. We provide evidence for the restored deformability of mature Stage V gametocytes. These results favour the idea that the change in shape and restored deformability are not random, but specifically designed to pass the spleen and traverse endothelial slits to allow their circulation. Further functional studies are required to explore this interesting hypothesis both on a mechanistic level and during human infection.

Experimental procedures

P. falciparum in vitro *culture*

Parasites of a gametocyte-producing clone, P2G12 (Buchholz *et al*., 2011), from the reference strain 3D7 were used in all experiments. The parental 3D7 line is a kind gift of Dr. Kim Williamson (Loyola University, Chicago). Cell culture of wild-type and transgenic lines was performed essentially as described (Trager and Jensen, 1976). Parasites were maintained in *in vitro* culture in fresh type 0+ human erythrocytes (Research Blood Components, LCC), suspended at 4% haematocrit in HEPES-buffered RPMI 1640 containing 10% serum (Interstate Blood bank), 0.5 ml gentamycin, 2.01 g sodium bicarbonate and 0.05 g hypoxanthine at pH 6.74. Cultures were kept at 37°C in a gassed chamber at 5% CO_2 and 1% O_2. For gametocyte production sorbitol synchronized ring-stage parasites were seeded at 1–2% parasitaemia into 75 cm^2 vented flasks at 6% haematocrit. Three days later the culture medium was doubled to trigger sexual conversion. Samples were taken over a 2-week period to obtain all gametocyte stages.

Plasmid construction and generation of transgenic parasites

To generate the plasmid 164/TdTomato, the coding sequence spanning the KAHRP signal sequence and GFPmut in the plasmid 164/GFP (Buchholz *et al*., 2011) was replaced with the coding sequence of TdTomato (Shaner *et al*., 2004), using the unique restriction enzyme sites NotI and MfeI. TdTomato was amplified from a plasmid containing the TdTomato ORF provided by the Tsien laboratory (University of California at San Diego, La Jolla, CA, USA). To generate a transgenic parasite line expressing TdTomato under the *PF10_0164* upstream sequence, 100 μg of purified 164/TdTomato plasmid DNA was transfected into P2G12 parasites at 5% ring stage parasitaemia, and transgenic parasites selected using 10 nM of the antifolate compound WR99210 (Jacobus Pharmaceuticals), as described (Wu *et al*., 1996).

Epifluorescence microscopy and 3D imaging

For epifluorescence images, live TdTomato expressing parasites were viewed at ambient temperature with a Axioscope M1 microscope (Zeiss, Jena Germany) equipped with a 100×/1.4 oil immersion lens and a Orca C4742-95 camera (Hamamatsu, Hamamatsu City Japan). Images were collected using the Zeiss Axiovision software.

For RBC membrane labelling, 100 μl of cells (at 5% haematocrit) was washed in phosphate-buffered saline (PBS) and incubated for 15 min in 100 μl of 5 μM Bodipy-FL-C_5-ceramide (Invitrogen) at 37°C. After labelling, cells were washed and resuspended in 200 μl of pre-warmed PBS before transferring them to the glass bottom of a sterile uncoated hydrophobic 35 mm Petri dish, which was pretreated with 0.5 mg ml^{-1} concavalin A (ConA, Sigma) as described previously (Gruring *et al*., 2011). Cells were allowed to settle and bind to ConA for 10 min, unbound cells were washed off using PBS and pre-warmed PBS was added to cover the bound cells. Immediately afterwards, cells were viewed using an Olympus FV1000 confocal microscope equipped with a 100×/1.4 oil immersion lens. Bodipy-FL-C_5-ceramide was excited with a 488 nm laser and TdTomato with a 559 nm. Images were acquired using Fluoview v1.7b (Olympus, Center Valley, PA, USA) using sequential detection. Stacks were collected using the following parameters: 4 μs dwell time, 512 × 512 dpi, 16–32 z-stacks. Three-dimensional images were constructed using the Imaris software 7.1.1 (Bitplane, Zurich Switzerland). Surface areas and volumes were calculated using isosurfaces that were manually created by tracing the contours in individual layers of the parasite or the host cell respectively. Each infected RBC (iRBC) was staged independently by three lab members using published criteria (Hawking *et al*., 1971; Sinden, 1982).

Micropipette aspiration experiments

Parasite cultures enriched by magnet purification were washed and resuspended in pre-warmed RPMI1640 containing 1% bovine serum albumin at a dilution of 5×10^5 cells ml^{-1}. The suspension was then injected into a sample chamber sitting on a heating stage (Linkam, Tadworth, UK) set at 37°C. A borosilicate glass micropipette was used to extract the iRBC membrane shear modulus and gametocyte elasticity (rigidity) by micropipette aspiration technique. The micropipette inner diameter was 1.9 ± 0.25 μm. A pressure drop rate of 1 Pa s^{-1} and a total pressure drop of 100 Pa were applied to aspirate and deform each cell. The cell membrane was monitored using a 100× immersion lens coupled with a 1.6× magnifier. Images were captured using an QColor5 High Resolution Color CCD Digital FireWire Camera

(Olympus) and processed by QCapture Pro 6.0 (Olympus). At the end of the aspiration procedure a fluorescent image was recorded documenting the parasite shape. Each infected RBC (iRBC) was staged independently by three lab members using published criteria (Hawking *et al.*, 1971; Sinden, 1982).

Modelling set-up and considerations

Mathematical description of iRBC and parasite shapes. Due to the highly irregular infected red blood cell (iRBC) shapes during the sexual development, applying classical micropipette theory for shear modulus evaluation is expected to introduce significant error. For more accurate extraction of the iRBC deformability, we built full three-dimensional finite element models for evaluating membrane and parasite rigidity through micropipette aspiration experiments using the commercial finite element method (FEM) package ABAQUS (SIMULIA, Providence, RI, USA). The modelling approach extended from earlier 3D FEM red blood cell models (Dao *et al.*, 2003; Mills *et al.*, 2004; Peng *et al.*, 2010). The geometries of the finite element models were generated by fitting the 3D reconstruction of the representative cells at different stages, as shown in Fig. 2A. We employ the following set of equations to describe the best fit for infected cell and parasite shapes for each stage:

$$y' = \pm\sqrt{1-\frac{4(x'^2+z'^2)}{W^2}}\left[\frac{L}{2}+a(x'^2+z'^2)+b(x'^2+z'^2)^2\right] \quad (1)$$

$$z = \frac{2z'}{W}(c+dx'+ex'^2+fx'^3+gx'^4+hx'^5) \quad (2)$$

$$x = R-\frac{\sqrt{R^2-\frac{L^2}{4}}}{\sqrt{R^2+y'^2-\frac{L^2}{4}}}(R-x') \quad (3)$$

$$y = \frac{y'}{\sqrt{R^2+y'^2-\frac{L^2}{4}}}(R-x') \quad (4)$$

where x, y, z are the final co-ordinates and x', y', z' are the transitional co-ordinates. Variables L and W are the length and width of the cell, and a, b, c, d, e, f, g, h are the coefficients to be fitted. Note that Eq. 1 has been used to describe the biconcave shape of healthy RBCs (Fung, 1993). Equation 2 is used to describe the thickness profile. The maximum value of polynomial $c+dx'+ex'^2+fx'^3+gx'^4+hx'^5$ is half of the cell thickness T. As we defined mature gametocytes by their curved shape, we used Eqs 3 and 4 for 'bending' transformations to describe this curved banana-like morphology. R is the curvature radius of the banana shape, and the average measured value of R is about 13 μm. For RBC shapes and other stage parasite shapes, we set $R=\infty$, which leads to $x=x'$, $y=y'$ in Eqs 3 and 4. The fitted coefficients for the cells shown in Fig. 3 are listed in Tables S1 and S2. The surface fitting tool in MATLAB is applied to fit these coefficients.

Shear modulus calculations. For the micropipette experiments, we simulate each individual cell using the stage-specific coefficients plus the specific parameters of each aspiration experiment (cell size, aspiration length, aspiration pressure and pipette diameter, Table S3). In addition, we also match the initial and maximum aspiration lengths of each micropipette experiment in the simulations. An iterative scheme is used to calibrate the shear modulus by comparing load-displacement aspiration curves between experiments and simulations.

Importantly, we simulate the aspiration experiments from different locations of the cells, specifically along the longitudinal direction (i.e. the aspiration from the iRBC head) and along the transverse direction (i.e. aspiration from the side). Due to the irregular geometry and the parasite orientation, the aspiration curve characteristics are different between head and side aspiration experiments. As shown in Fig. 3, assuming nominally uniform shear modulus of the iRBC membrane, the parasite rigidity can be estimated from comparing the different aspiration curves from cell head and cell side. For this purpose, we first calibrate the iRBC membrane shear modulus by ignoring the influence of the parasite. Parametric simulations and experimental fluorescence images show that parasite rigidity has little influence when iRBCs are aspired from the side, but becomes significant when iRBCs are aspired from the head. Thus, assuming the extracted shear modulus from the iRBC side represents the 'true' membrane shear modulus, we can estimate the parasite rigidity using the aspiration data from the iRBC head by modelling the parasite as a homogeneous solid and matching the aspiration curve. The parasite rigidity estimation is carried out using average cell and parasite dimensions and average membrane shear modulus calibrated from experiments.

Material constitutive laws. In the parasite rigidity estimation, we model the parasite as a neo-Hookean nearly incompressible hyperelastic material. The interaction between the host cell membrane and the parasite, and the interaction between cell membrane and pipette inner surface are modelled as frictionless surface-to-surface contact. We model the host RBC membrane as the Evans-Skalak hyperelastic material. It is written as

$$T_1 = K(\lambda_1\lambda_2-1)+\frac{\mu}{2\lambda_1^2\lambda_2^2}(\lambda_1^2-\lambda_2^2), \quad (5)$$

$$T_2 = K(\lambda_1\lambda_2-1)+\frac{\mu}{2\lambda_1^2\lambda_2^2}(\lambda_2^2-\lambda_1^2), \quad (6)$$

where T_1 and T_2 are the principal stress resultants, λ_1 and λ_2 are the principal stretches, and K and μ are the area and shear moduli of the membrane. We employ S4R/S4 shell elements to model the membrane. Membrane thickness is given as 2.2 nm and $K=5\times10^5$ *pN*/*μm*. The discrepancy between the membrane thickness used herein and its actual value (4–5 nm) is attributed to the fact that in our study the membrane is simplified as a continuous (but anisotropic) shell without considering its detailed molecular architecture (see Peng *et al.*, 2010). The bending stiffness is given as 2×10^{-19} *J*. A material user subroutine VUMAT is developed to implement Eqs 5 and 6. A surface-based cavity model is applied to enforce cell volume conservation.

Shear modulus calibration procedure. By fitting the experimental curve, we first make an initial guess of the membrane shear modulus based on the classical micropipette aspiration theory, i.e. hemispherical cap model, and we use it as an input for the finite element model to carry out the simulation and obtain the aspiration curve. Because the classical micropipette aspiration theory is not accurate for the gametocytes, the simulation aspiration curve obtained using the initial shear modulus is different from the experimental aspiration curve. Based on the difference, we adjust the shear modulus, and carry out another simulation to

obtain a new curve, and compare the slopes again. We repeat the simulations iteratively until the curve slopes between the experiments and simulations are close enough. Finally, the shear modulus we used for the finite element model converges to a value, which is the ultimate calibrated shear modulus value. During this procedure, the initial and final aspiration lengths are matched between simulations and experiments.

Parasite rigidity estimation procedure. The shear modulus calibration results show that the membrane shear modulus predicted through head-on experiment is always higher than the value predicted through side-on experiment. This can be explained by the effect of the parasite. Both micropipette experiments with fluorescence imaging and FEM simulation show that the parasite plays a significant role in head-on aspiration while its influence is negligible for aspiration from the side. Then, we can estimate the parasite rigidity based on the difference of the predicted average shear modulus values between head-on and side-on aspirations. We consider the membrane shear modulus predicted through side-on aspirations as the true membrane shear modulus, while the shear modulus predicted through head-on aspiration is the membrane shear modulus plus the parasite influence. We model the parasite as an elastic homogeneous solid. Using the average geometries of iRBCs and parasites in each stage, we carry out two sets of simulations. In the first set, we simulate the cell aspirated into the pipette from the head with parasite inside modelled as a solid body. The membrane shear modulus for this simulation is the average value obtained from side-on aspirations, which we assume is the true membrane shear modulus. In the second set, we simulate the same cell aspirated from the head, but without parasite inside (membrane only). The membrane shear modulus used is the average value obtained from the head-on shear modulus calibration. Then we match the curve slopes of these two sets of simulations by adjusting the parasite rigidity in the first set iteratively to estimate the parasite rigidity.

Modelling splenic passage and microcirculation of iRBCs. After obtaining the membrane shear modulus and parasite rigidity, we can study the critical conditions of gametocytes passing the splenic endothelial slits. The length of the splenic slit is estimated to be ~ 2 μm, the distance between the annular fibres is estimated to be ~ 3–4 μm, and the slit width is estimated to be ~ 1–2 μm (Cokelet, 1981; Deplaine *et al*., 2011). In our simulations, the length of the slit is given as 2 μm, the distance between the annular fibres varies from 3 to 4 μm, and the slit width varies from 1.5 to 2 μm. The pressure is applied on the front half body of the red blood cells. Similar set-up was used in the simulations of the critical conditions of iRBCs passing through smallest capillaries in microcirculation. The diameter of the capillaries we studied here varies from 3.5 to 4.5 μm.

Acknowledgements

The authors thank Vagheesh Narasimhan for help with the statistical analysis of vital parameters and shear modulus data, and Christof Gruering for technical help with 3D imaging. This work was supported by NIH grants R01A107755801 (M.M.) and R01HL094270 (Z.L.P., M.D.S., M.D., S.S.), and by the Infectious Diseases Interdisciplinary Research Group of the Singapore MIT Alliance for Research and Technology (SMART) (Z.L.P., M.D.S., C.T.L., M.D., S.S.), and the Advanced Materials for Micro and Nano Systems Programme of the Singapore-MIT Alliance (SMA) (R.Z., C.T.L., M.D., S.S.). One of the authors (A.U.) gratefully acknowledges support by the Alexander von Humboldt-Foundation in form of a Feodor Lynen Research Fellowship.

References

Bachmann, A., Esser, C., Petter, M., Predehl, S., von Kalckreuth, V., Schmiedel, S., *et al*. (2009) Absence of erythrocyte sequestration and lack of multicopy gene family expression in *Plasmodium falciparum* from a splenectomized malaria patient. *PLoS ONE* **4:** e7459.

Buchholz, K., Burke, T.A., Williamson, K.C., Wiegand, R.C., Wirth, D.F., and Marti, M. (2011) A high-throughput screen targeting malaria transmission stages opens new avenues for drug development. *J Infect Dis* **203:** 1445–1453.

Cokelet, G.R. (1981) Dynamics of erythrocyte motion in filtration tests and *in vivo* flow. *Scand J Clin Lab Invest Suppl* **156:** 77–82.

Dao, M., Lim, C.T., and Suresh, S. (2003) Mechanics of the human red blood cell deformed by optical tweezers. *J Mech Phys Solids* **51:** 2259–2280.

David, P.H., Hommel, M., Miller, L.H., Udeinya, I.J., and Oligino, L.D. (1983) Parasite sequestration in *Plasmodium falciparum* malaria: spleen and antibody modulation of cytoadherence of infected erythrocytes. *Proc Natl Acad Sci USA* **80:** 5075–5079.

Dearnley, M.K., Yeoman, J.A., Hanssen, E., Kenny, S., Turnbull, L., Whitchurch, C.B., *et al*. (2012) Origin, composition, organization and function of the inner membrane complex of *Plasmodium falciparum* gametocytes. *J Cell Sci* (in press).

Deplaine, G., Safeukui, I., Jeddi, F., Lacoste, F., Brousse, V., Perrot, S., *et al*. (2011) The sensing of poorly deformable red blood cells by the human spleen can be mimicked *in vitro*. *Blood* **117:** e88–e95.

Diez-Silva, M., Dao, M., Han, J.Y., Lim, C.T., and Suresh, S. (2010) Shape and biomechanical characteristics of human red blood cells in health and disease. *MRS Bull* **35:** 382–388.

Esposito, A., Choimet, J.B., Skepper, J.N., Mauritz, J.M., Lew, V.L., Kaminski, C.F., and Tiffert, T. (2010) Quantitative imaging of human red blood cells infected with *Plasmodium falciparum*. *Biophys J* **99:** 953–960.

Fung, Y.C. (1993) *Biomechanics: Mechanical Properties of Living Tissues*. New York: Springer.

Glenister, F.K., Coppel, R.L., Cowman, A.F., Mohandas, N., and Cooke, B.M. (2002) Contribution of parasite proteins to altered mechanical properties of malaria-infected red blood cells. *Blood* **99:** 1060–1063.

Gruring, C., Heiber, A., Kruse, F., Ungefehr, J., Gilberger, T.W., and Spielmann, T. (2011) Development and host cell modifications of *Plasmodium falciparum* blood stages in four dimensions. *Nat Commun* **2:** 165.

Handayani, S., Chiu, D.T., Tjitra, E., Kuo, J.S., Lampah, D., Kenangalem, E., *et al*. (2009) High deformability of *Plasmodium vivax*-infected red blood cells under microfluidic conditions. *J Infect Dis* **199:** 445–450.

Hanssen, E., Knoechel, C., Dearnley, M., Dixon, M.W., Le Gros, M., Larabell, C., and Tilley, L. (2011) Soft X-ray

microscopy analysis of cell volume and hemoglobin content in erythrocytes infected with asexual and sexual stages of *Plasmodium falciparum*. *J Struct Biol* **177:** 224–232.
Hawking, F., Wilson, M.E., and Gammage, K. (1971) Evidence for cyclic development and short-lived maturity in the gametocytes of *Plasmodium falciparum*. *Trans R Soc Trop Med Hyg* **65:** 549–559.
Hayward, R.E., Tiwari, B., Piper, K.P., Baruch, D.I., and Day, K.P. (1999) Virulence and transmission success of the malarial parasite *Plasmodium falciparum*. *Proc Natl Acad Sci USA* **96:** 4563–4568.
Krause, W.J. (2005) *Krause's Essential Human Histology for Medical Students*. Boca Raton: Universal Publisher.
Maier, A.G., Rug, M., O'Neill, M.T., Brown, M., Chakravorty, S., Szestak, T., *et al*. (2008) Exported proteins required for virulence and rigidity of *Plasmodium falciparum*-infected human erythrocytes. *Cell* **134:** 48–61.
Mills, J.P., Qie, L., Dao, M., Lim, C.T., and Suresh, S. (2004) Nonlinear elastic and viscoelastic deformation of the human red blood cell with optical tweezers. *Mech Chem Biosystems* **1:** 169–180.
Mills, J.P., Diez-Silva, M., Quinn, D.J., Dao, M., Lang, M.J., Tan, K.S., *et al*. (2007) Effect of plasmodial RESA protein on deformability of human red blood cells harboring *Plasmodium falciparum*. *Proc Natl Acad Sci USA* **104:** 9213–9217.
Murray, C.J., Rosenfeld, L.C., Lim, S.S., Andrews, K.G., Foreman, K.J., Haring, D., *et al*. (2012) Global malaria mortality between 1980 and 2010: a systematic analysis. *Lancet* **379:** 413–431.
Nash, G.B., O'Brien, E., Gordon-Smith, E.C., and Dormandy, J.A. (1989) Abnormalities in the mechanical properties of red blood cells caused by *Plasmodium falciparum*. *Blood* **74:** 855–861.
Park, Y., Diez-Silva, M., Popescu, G., Lykotrafitis, G., Choi, W., Feld, M.S., and Suresh, S. (2008) Refractive index maps and membrane dynamics of human red blood cells parasitized by *Plasmodium falciparum*. *Proc Natl Acad Sci USA* **105:** 13730–13735.
Peng, Z.L., Asaro, R.J., and Zhu, Q. (2010) Multiscale simulation of erythrocyte membranes. *Phys Rev E* **81:** 031904 1–11.
Rogers, N.J., Daramola, O., Targett, G.A., and Hall, B.S. (1996) CD36 and intercellular adhesion molecule 1 mediate adhesion of developing *Plasmodium falciparum* gametocytes. *Infect Immun* **64:** 1480–1483.
Shaner, N.C., Campbell, R.E., Steinbach, P.A., Giepmans, B.N., Palmer, A.E., and Tsien, R.Y. (2004) Improved monomeric red, orange and yellow fluorescent proteins derived from *Discosoma* sp. red fluorescent protein. *Nat Biotechnol* **22:** 1567–1572.
Silvestrini, F., Bozdech, Z., Lanfrancotti, A., Di Giulio, E., Bultrini, E., Picci, L., *et al*. (2005) Genome-wide identification of genes upregulated at the onset of gametocytogenesis in *Plasmodium falciparum*. *Mol Biochem Parasitol* **143:** 100–110.
Silvestrini, F., Lasonder, E., Olivieri, A., Camarda, G., van Schaijk, B., Sanchez, M., *et al*. (2010) Protein export marks the early phase of gametocytogenesis of the human malaria parasite *Plasmodium falciparum*. *Mol Cell Proteomics* **9:** 1437–1448.
Sinden, R.E. (1982) Gametocytogenesis of *Plasmodium falciparum in vitro*: ultrastructural observations on the lethal action of chloroquine. *Ann Trop Med Parasitol* **76:** 15–23.
Smalley, M.E., Abdalla, S., and Brown, J. (1981) The distribution of *Plasmodium falciparum* in the peripheral blood and bone marrow of Gambian children. *Trans R Soc Trop Med Hyg* **75:** 103–105.
Spielmann, T., Fergusen, D.J., and Beck, H.P. (2003) etramps, a new *Plasmodium falciparum* gene family coding for developmentally regulated and highly charged membrane proteins located at the parasite-host cell interface. *Mol Biol Cell* **14:** 1529–1544.
Suresh, S., Spatz, J., Mills, J.P., Micoulet, A., Dao, M., Lim, C.T., *et al*. (2005) Connections between single-cell biomechanics and human disease states: gastrointestinal cancer and malaria. *Acta Biomater* **1:** 15–30.
Thomson, J.G., and Robertson, A. (1935) The structure and development of *Plasmodium falciparum* gametocytes in the internal organs and peripheral circulation. *Trans R Soc Trop Med Hyg* **14:** 31–40.
Trager, W., and Jensen, J.B. (1976) Human malaria parasites in continuous culture. *Science* **193:** 673–675.
Waugh, R.E., Narla, M., Jackson, C.W., Mueller, T.J., Suzuki, T., and Dale, G.L. (1992) Rheologic properties of senescent erythrocytes: loss of surface area and volume with red blood cell age. *Blood* **79:** 1351–1358.
Wu, Y., Kirkman, L.A., and Wellems, T.E. (1996) Transformation of *Plasmodium falciparum* malaria parasites by homologous integration of plasmids that confer resistance to pyrimethamine. *Proc Natl Acad Sci USA* **93:** 1130–1134.

Supporting information

Additional Supporting Information may be found in the online version of this article:

Table S1. Coefficients of fitting equations for the infected RBCs.
Table S2. Coefficients of fitting equations for the parasites.
Table S3. Dimension measurement, surface area and volume of infected red blood cells and parasites at different sexual stages.
Supporting Videos. 15 supplementary video files (S4–S18) are provided. For each gametocyte stage, including male and female mature gametocytes, three videos are included that show a representative cell in 3D. The first shows a 3D reconstruction of the parasite by TdTomato fluorescence, the second shows the host cell labelled with Bodipy-FL5-Ceramide, and the third one shows 3D reconstruction with isosurfaces for both parasite and host cell, based on their respective fluorescence stain.

Please note: Wiley-Blackwell are not responsible for the content or functionality of any supporting materials supplied by the authors. Any queries (other than missing material) should be directed to the corresponding author for the article.